Published in final edited form as:
Cell Mol Bioeng. 2008 December 1; 1(4): 276–288. doi:10.1007/s12195-008-0024-8.

Measuring Receptor–Ligand Binding Kinetics on Cell Surfaces: From Adhesion Frequency to Thermal Fluctuation Methods

Wei Chen[1], **Veronika I. Zarnitsyna**[2], **Krishna K. Sarangapani**[1,2], **Jun Huang**[2], and **Cheng Zhu**[1,2]

[1]Woodruff School of Mechanical Engineering, Georgia Institute of Technology, Atlanta, GA 30332, USA

[2]Coulter Department of Biomedical Engineering, Georgia Institute of Technology, Atlanta, GA 30332, USA

Abstract

Interactions between surface-anchored receptors and ligands mediate cell–cell and cell–environment communications in many biological processes. Molecular interactions across two apposing cell membrane are governed by two-dimensional (2D) kinetics, which are physically distinct from and biologically more relevant than three-dimensional (3D) kinetics with at least one interacting molecular species in the fluid phase. Here we review two assays for measuring 2D binding kinetics: the adhesion frequency assay and the thermal fluctuation assay. The former measures the binding frequency as a function of contact duration and extracts the force-free 2D kinetics parameters by nonlinearly fitting the data with a probabilistic model. The latter detects bond formation/dissociation by monitoring the reduction/resumption of thermal fluctuations of a force sensor. Both assays are mechanically based and operate at the level of mostly single molecular interaction, which requires ultrasensitive force techniques. Characterization of one such technique, the biomembrane force probe, is presented.

Keywords

Adhesion frequency assay; Thermal fluctuation assay; Micropipette; Biomembrane force probe; Kinetics; Receptor–ligand interaction

Introduction

Communication between cells with each other and with their environment is mediated via specific receptors on their surfaces. Although unraveled genome for key organisms has provided a lot of information about different surface molecules as corresponding gene products, only a fraction of them have functions assigned and even fewer have been studied in detail. Traditionally, receptor–ligand interactions are characterized by ensemble assays with at least one of the molecules purified from the cell membrane. The assays are carried out in the fluid phase, e.g., using the surface plasmon resonance technique. These are referred to as three-dimensional (3D) assays and are described in terms of a chemical reaction framework through receptor and ligand concentrations, kinetic rates, and binding affinity. While sufficient for a proper description in homogeneous solution, these properties by themselves are often insufficient for determining the interaction of the same molecules residing in their natural

Address correspondence to Cheng Zhu, Coulter Department of Biomedical Engineering, Georgia Institute of Technology, Atlanta, GA 30332, USA. cheng.zhu@bme.gatech.edu.

environment on the cell membrane. This is because cell surface molecules can be clustered, partitioned in cell surface structures such as membrane rafts, or linked to cytoskeleton directly or via other docking molecules, which can impact binding by signaling that changes molecular conformations. On the cell, molecules of interest may be abundant but inactive due to specific cellular environment or the same molecules may exhibit different activities in different areas or times. These features make ensemble assays insufficient, even if they are carried out on the cell surface, because the properties so measured represent ensemble averages only. It also calls for single molecule studies because these experiments probe molecular interactions one by one, thereby allowing for measurement of not only average properties but also their distributions.

Another important feature of receptor-mediated cell adhesion is that molecular interactions take place in two dimensions (2D) as both receptors and ligands are anchored to the respective surfaces of two apposing cells or a cell and a substrate. This situation is ideal for single-molecule force techniques because the sensitive force probes can be functionalized with interacting molecules. A molecular interaction manifests as a mechanical force through a receptor-ligand bond that physically connects two surfaces, one of which can be the force probe (the other is referred to as the target surface in this paper). Single-molecule biomechanical experiments with atomic force microscopy (AFM) or other ultrasensitive force techniques for measuring unbinding forces for dynamic force spectroscopy analysis or unfolding of protein domains are discussed in other papers of this thematic issue. In this review, we summarize our previous work that uses an adhesion frequency assay[2] and a thermal fluctuation assay[1] to extract kinetic information of receptor–ligand interaction from measured binding events.

Adhesion Frequency Assay

The simplest mechanical measurement is the detection of the presence of adhesion mediated by specific receptor–ligand bond(s) at a given time, regardless of how many bonds are involved, how long they last, and how big a force is required to detach the adhesion. It is desirable, but not required, that the observed adhesion is mediated by a single bond. To achieve single-bond measurement requires the use of a force probe with sufficient sensitivity for single-bond detection and experimental conditions that limit multi-bond interactions, e.g., using low site densities (compared to the 2D K_d) of receptors and ligands on the respective surfaces such that binding events become rare, which is a necessary but not a sufficient condition.[19] There is also no need for a quantitative measurement of the rupture force required to detach the adhesion (when adhesion is present). It suffices to determine qualitatively whether an adhesion is present. In the original adhesion frequency assay,[2] the adhesion sensor used was a human red blood cell (RBC) aspirated by a micropipette via a small suction pressure (Fig. 1), which was previously used by Evans and coworker to measure piconewton-level adhesion forces.[3] Here, the sensor precision for the force measurement is not a requirement because adhesion can be visualized microscopically from the elongation of RBC membrane (Fig. 1c). But its sensitivity is important because insufficient sensitivity would miss adhesion events mediated by weak interactions, thereby underestimating the adhesion frequency (below). The ability of the aspirated RBC sensor to detect weak interactions will be demonstrated in section “Characterization of BFP” where the BFP calibration is discussed.

Although this simplest measurement produces only a random binary readout of either adhesion (scored 1) or no adhesion (scored 0), it can be used to estimate the probability of adhesion, e.g., from the frequency of adhesion, i.e., the average of adhesion scores from repeated measurements. When adhesion becomes infrequent and requires a probabilistic description for its presence, the number of molecular bonds that mediate adhesion must be low and should follow a Poisson distribution[10]:

$$p_n = \frac{\langle n \rangle^n}{n!} \exp(-\langle n \rangle), \tag{1}$$

where p_n is the probability of having n bonds and $\langle n \rangle$ is the average number of bonds, which can be smaller than 1 under infrequent adhesion condition. The probability of adhesion P_a is:

$$P_a = 1 - p_0 = 1 - \exp(-\langle n \rangle). \tag{2}$$

The average number of bonds is a statistic equivalent to the density of bonds, which increases with increasing densities of receptors and ligands due to mass action and changes during a kinetic process depending on time and the kinetic rate constants. For a second-order forward, first-order reverse, single-step bimolecular interaction,

$$R + L \underset{k_{-1}}{\overset{k_{+1}}{\rightleftharpoons}} B, \tag{3}$$

where R, L, and B denote, respectively, the receptor, ligand, and bond, and k_{+1} and k_{-1} denotes the respective on- and off-rate constants, $\langle n \rangle$ obeys the following kinetic equation and initial condition:

$$\frac{d\langle n \rangle}{dt_c} = m_r m_l A_c k_{+1} - k_{-1} \langle n \rangle \quad \text{and} \quad \langle n \rangle \Big|_{t_c=0} = 0, \tag{4}$$

where A_c is the contact area and t_c is the contact duration, m_r and m_l are receptor and ligand surface densities, respectively. The solution is:

$$\langle n \rangle = m_r m_l A_c K_a \left[1 - \exp(-k_{-1} t_c)\right], \tag{5}$$

where $K_a = k_{+1}/k_{-1}$ is the binding affinity. Substituting Eq. (5) into Eq. (2) yields[2]

$$P_a = 1 - \exp\left\{-m_r m_l A_c K_a \left[1 - \exp(-k_{-1} t_c)\right]\right\}. \tag{6}$$

Unlike 3D assays where soluble molecules in the fluid phase can diffuse to the vicinity of the counter-molecules, 2D assay requires that the force probe and the target surface be brought into contact because interaction would not be physically possible if the two surfaces are separated by distances greater than the span of the receptor–ligand complex. Thus, the initiation of interaction is, in a sense, "staged" by the experimenter who puts the two surfaces into contact, controls the area and duration of the contact, and observe the outcome of such an adhesion test at the end of the contact when the two surfaces are separated.

To estimate P_a from the average adhesion score in a series of repeated contact–separation cycle (called adhesion test cycle) requires that the parameters on the right-hand side of Eq. (6) be constants. In the micropipette adhesion frequency assay,[2] the adhesion test cycle is controlled via computer-driven micromanipulation to ensure each contact is as close to identical to any other contacts as possible to yield constant A_c and t_c. The "apparent" contact area A_c^* can be visualized microscopically, as shown in the side view photomicrograph of Fig. 1b. However,

the functional contact area A_c depends on the microtopology of the cell surface.[14] Furthermore, making a contact is a process that starts from a point to the final area, which requires time (termed lead time). Similarly, separating a finite contact and stretching the RBC membrane to the point when visual detection can be reliably made is also a process that requires time (termed dead time). It is implied in the derivation of Eq. (6) that the sum of these times is much smaller than t_c such that the lead time and dead time are negligible during the course of a test cycle. This requirement places a limitation to the temporal resolution of the assay such that the half-life of the molecular interaction in question has to be much longer than the sum of lead time and dead time.[2]

The molecular densities m_r and m_l are usually assumed constant because the contact time t_c (<1 min) is much shorter than the time t_d required to recruit molecules into the apparent contact area $A_c^*(\sim 3\,\mu m^2)$ from outside by diffusion. Indeed, for a typical diffusion coefficient $D \sim 0.01$ $\mu m^2/s$ of cell surface molecules t_d can be estimated as $A_c^*/D \sim 5$ min.[13] However, this assumption will be invalid if engagement of receptors by their adhesive ligands triggers cell signaling that results in reorganization of cell surface structures, such as changes in clustering of receptors and/or their partitioning in membrane microdomains. Signaling can also alter the kinetic rates and binding affinity, thereby violating the assumption of constant K_a, k_{-1}, and/or k_{+1}. These events can occur in short time, thereby complicating the analysis and interpretation of the adhesion score sequence measured from the adhesion frequency assay. In fact, a recent study has demonstrated that the adhesion probability of a test cycle in a repeated test series may depend on the outcome of the prior test(s) in the sequence.[18] All three possible cases have been observed: the adhesion probability of the next test can be increased (positive memory), decreased (negative memory), or unchanged (no memory) by the adhesion of the immediate past test. The underlying causes of the memory effects are not clear, but may involve signaling that transiently changes the surface organization of the interacting molecules and/or their binding affinity.

Returning to the simple case with constant parameters, Eq. (6) states that the likelihood of observing adhesion, P_a, depends on the time when the observation is made relative to the time when the contact is initiated, i.e., the contact duration, t_c. If the adhesion frequency is measured over a range of contact durations, fitting Eq. (6) to the measured P_a vs. t_c binding curve then allows estimation of the 2D kinetic rates and binding affinity, provided that the receptor and ligand densities are measured from independent experiments.

Two sets of example data of the adhesion frequency assay for measuring 2D binding kinetics are shown in Fig. 2. Figure 2a shows P_a vs. t_c data of CD8, a coreceptor expressed on T lymphocytes from monoclonal T cell receptor (TCR) transgenic mice, interacting with a noncognate peptide bound to mouse major histocompatibility complex (pMHC) molecule coated on the surface of a human red blood cell (RBC).[5] Note that a single set of kinetics parameters enable the model to best fit the data with varied surface densities of receptors and ligands.

Although the adhesion frequency assay was originally proposed using the micropipette technique (Fig. 1), [2] it can be implemented using other ultrasensitive force techniques, such as optical tweezers,[12] biomembrane force probe (BFP, Fig. 3), [1] and AFM. As another example, Fig. 2b shows P_a vs. t_c data of L- or P-selectin reconstituted in glass-supported lipid bilayer[6] interacting with endoglycan-Ig chimeric molecule captured on the AFM cantilever tip by protein G.[11] In these experiments, the protein G-coated AFM cantilever was driven into (approach phase) and out of contact (retraction phase) with the selectin-incorporated bilayers using a piezo actuator. The deflection of the cantilever was continually monitored using a laser beam-bounce technique. An adhesion event was characterized by the visible bending of the cantilever during the retraction phase, leading to a force build-up. Followed by the raising force

is the eventual dissociation of the bond, causing the cantilever to snap back to zero mean force position, as signified by the precipitous drop of the force curve (cf. Fig. 7a). The contact area size A_c can be controlled by keeping the compressive force of the cantilever tip pressing against the bilayer the same for all contacts. When the force sensor involves RBCs or microspheres as in the cases of micropipette, optical tweezers, and BFP, the surface densities of the molecules can be determined by flow cytometry using fluorescently labeled monoclonal antibodies against the molecules. By comparison, it is more difficult to measure the site density on an AFM cantilever, especially on the sharp tip with a radius of curvature of ~50 nm. Hence, an adhesion frequency experiment using AFM would only give us a "lumped" value for $m_r m_l A_c K_a$ but not the individual values.

Characterization of BFP

The thermal fluctuation assay, to be discussed in the next section, requires an ultrasensitive force sensor with a soft spring (the spring constant should be smaller than those of the interacting molecules), such as a BFP or optical tweezers. A BFP is a high-tech version of a micropipette, which includes a probe bead glued to the apex of the micropipette-aspirated RBC as a picoforce transducer (Fig. 3, left). Observed under an inverted microscope (Zeiss Axiovert 100 with 40× objective and 4× video tube), the position of the probe bead is tracked by a high-speed camera (1,500 frames per second, Cooke SensiCam) with customized and advanced image analysis software to achieve high spatial precision. In order to achieve high frame rates, the high-speed camera only captures a narrow strip of the field of view (1024 × 27 pixels), which is binned into a single line. This line is then transferred from the camera to the computer to carry out the online image analysis to determine the darkest position of the left edge of the probe bead (Fig. 3). A target bead (or cell) is aspirated by an apposing micropipette (Fig. 3, right) driven by a computer-controlled piezo translator (Physik Instrument).

Since our BFP was custom-designed by Dr. Evan Evans, who helped us assemble it in our laboratory, we first present characterization of our BFP apparatus in this section. To determine the spatial precision of our BFP (Fig. 3), we compared the displacements of the target bead tracked by the image tracking system (Fig. 4a, red circles, left ordinate) with the displacements of piezo translator that drove the right pipette on which the target bead was aspirated (Fig. 4a, green squares, left ordinate). The piezo translator used an integrated capacitive feedback control to achieve sub-nanometer spatial precision and was programmed to travel back and forth in a quasi-rectangular waveform. It is evident that the tracked displacements followed the programmed displacements very well (Fig. 4a). The differences between the two (Fig. 4a, blue triangles, right ordinate) were analyzed by histogram (Fig. 4b), which follows a Gaussian distribution with a standard deviation of ~3 nm. This analysis establishes that the spatial precision of our image tracking system is ±3 nm.

Both the simple micropipette system (Fig. 1) and the more sophisticated BFP (Fig. 3) use a pressurized RBC as an ultrasensitive force transducer. The 3-nm spatial precision of the BFP's image tracking system can be translated to sub-piconewton force sensitivity by multiplying the axial deflection of the RBC force transducer by its "spring constant", k_p. Several approximate expressions for k_p have been derived based on membrane mechanics, for example, the equation by Evans *et al.*[4] reads

$$k_p \approx \frac{\pi R_p \Delta_P}{(1 - R_p/R_0) \ln \left[4R_0^2/(R_p R_c)\right]}, \tag{7}$$

where Δp is the suction pressure and R_p, R_0, and R_c are the respective radii of the pipette lumen, the spherical portion of the aspirated RBC, and the adhesive contact between the RBC and the probe bead (cf. Fig. 3).

Calibration of the BFP spring constant can be done using thermal fluctuation analysis, which is based on the equipartition theorem,

$$\frac{1}{2}k_p \mathrm{var}(X)=\frac{1}{2}k_B T, \tag{8}$$

where var(X) is the variance of the thermally excited random displacements X of the force probe, k_B is the Boltzmann constant, and T is the absolute temperature. Figure 5 compares the time courses of displacements of the target bead (Fig. 5a), the probe bead (Fig. 5b), and the left pipette mouth on which the RBC was mounted (Fig. 5c) while the two pipettes were held stationary. It is evident that the force probe displacements exhibit significantly larger fluctuations than those of the other two sites, indicating that the large fluctuations are caused by thermal excitation of the force probe confined by a very soft spring.

Due to the finite temporal resolution (limited by the camera speed), the measured displacements X_m are an average of X over the time window during which a single frame of image is acquired. This causes a so-called "motion-blur" effect, as discussed by Wong and Halvorsen[15] and references therein, that reduces the measured variance var(X_m) from var(X) by a factor of $S(\alpha)$, i.e.,

$$\mathrm{var}(X)=\mathrm{var}(X_m)S^{-1}(\alpha). \tag{9}$$

S(α) is the motion-blur correction function,[15]

$$S(a)=\frac{2}{\alpha}-\frac{2}{\alpha^2}[1-\exp(-\alpha)], \tag{10}$$

where a is the ratio of the camera exposure time to the characteristic fluctuation time of the BFP, represented by the ratio of its spring constant to its friction coefficient. Thus, $\alpha = Ak_p$ where A is proportional to the camera exposure time but inversely proportional to the BFP friction coefficient. Since $k_p = C\Delta p$ from Eq. (7), it follows from substituting Eqs. (8) and (10) into Eq. (9) that

$$\mathrm{var}(X_m)=\frac{k_B T}{C\Delta_p}\left\{\frac{2}{AC\Delta_p}-\frac{2}{(AC\Delta_p)^2}[1-\exp(-AC\Delta_p)]\right\}. \tag{11}$$

To correct for low frequency drifts, we calculated a series of var(X_m) values after passing the displacement data through a series of high-pass filters and extrapolated the "drift-free" variance from the var(X_m) vs. filter frequency plot.[15]

Two sets of drift-free var(X_m) were plotted vs. $1/\Delta p$, one measured in hypotonic condition (Fig. 6a) and the other in isotonic condition (Fig. 6b). As expected, the var(X_m) of the force probe increased as the suction pressure decreased. By comparison, the control var(X_m) measured from the target bead and the left pipette mouth did not response to the changes of the suction pressure and was very small (<2 nm^2), indicating a very low noise level of our system. Equation (11) was nonlinearly fit to the background-subtracted var(X_m) vs. $1/\Delta p$ data, which returns two

parameters, A and C. This allows for calculation of the corrected var(X) from var(X_m) using Eqs. (9) and (10) with $\alpha = AC\Delta p$, which is plotted vs. $1/k_p$ calculated from Eq. (7) for hypotonic (Fig. 6c) and isotonic (Fig. 6d) conditions. Both data sets display a linear trend, as predicted by Eq. (8). The linear fit to the data in Fig. 6c has a slope of 4.0 pN-nm, in excellent agreement with the k_BT value at room temperature, supporting the validity of Eq. (7) in the hypotonic condition. By comparison, fitting the data in Fig. 6d with a straight line returns a slope of 2.5 pN-nm, significantly smaller than the 4.1 pN-nm value predicted by the equipartition theorem, suggesting that Eq. (7) is not valid in the isotonic condition. The assumptions underlying the analysis that yield Eq. (7) are reasonable when the RBC is swelled in hypotonic medium and forms a sphere after being aspirated by a pipette of 2–3 μm inner diameter to form a short cell tongue inside the pipette (cf. Fig. 3). These assumptions break down when isotonic medium is used. RBCs have a biconcave discoid shape in isotonic medium. To form a sphere from part of the cell requires the use of a smaller pipette to aspirate the rest of the cell into the pipette to form a much longer cell tongue, which greatly increases the friction between the pipette wall and the cell membrane, invalidating the frictionless assumption required for the analysis. Nevertheless, we should still be able to directly use the value C obtained by fitting Eq. (11) to Fig. 6b to calculate $k_p = C\Delta p$ for the spring constant for a BFP in the isotonic condition.

Thermal Fluctuation Assay

The adhesion frequency assay discussed in section “Adhesion Frequency Assay” extracts kinetic information from the dependence of adhesion frequency P_a on contact duration t_c.[2] Adhesion is measured mechanically by separating the force probe (pressurized RBC or AFM cantilever) from the target to detect the presence of a receptor–ligand bond or bonds that connect the two surfaces at the end of a contact but not when a bond forms or dissociates during the contact. Therefore, kinetics of molecular interaction must be inferred from fitting a model, e.g., Eq. (6), to the P_a vs. t_c data (Fig. 2).[2] By comparison, a recently developed thermal fluctuation assay can pinpoint the association and dissociation events at the single-bond level during the contact period without separating the two surfaces.[1] This greatly enhances the quantity, quality, and reliability of the information obtained, which makes kinetic measurements much simpler and more robust.

The idea of the thermal fluctuation assay is as follows. Due to their ultrasensitivity, force probes used for single-molecule experiments are usually susceptible to thermal fluctuations, as discussed in the preceding section (cf. Fig. 5). Formation of a molecular bond spanning across the gap between the force probe and the target physically connects the two surfaces together, which reduces the thermal fluctuation of the force probe. This is because bond formation adds mechanically the molecular spring k_m to the force probe spring k_p, thereby giving rise to a stiffer system spring k_s that is equivalent to two springs in parallel[16]:

$$k_s = k_p + k_m. \tag{12}$$

Indeed, this idea has been employed to measure the molecular elasticity of P- and L-selectins from the decreased thermal fluctuations of an AFM cantilever due to bond formation.[7] In this work, the AFM cantilevers have a nominal spring constant of $k_p \approx 10$ pN/nm and the molecular spring constants are $k_m \approx 1$ and 4 pN/nm for P- and L-selectins, respectively.[7] Adding a molecular spring constant of this magnitude in parallel to the cantilever spring constant results in a 10–40% increase in the system spring constant and a 10–40% decrease in the thermal fluctuations. This is shown in Fig. 7 where cantilever deflection vs. time (Figs. 7a, b), 15-point sliding standard deviation of the cantilever deflection vs. time (Figs. 7c, d), and their corresponding histograms (Figs. 7e, f) for L-selectin (Figs. 7a, c, e) and P-selectin (Figs. 7b, d, f), are respectively shown. The differences in the deflection fluctuations (as directly

visualized or measured by sliding standard deviations) between the free and bound cantilevers are more distinct for L-selectin (Figs. 7a, c) than for P-selectin (Figs. 7b, d). Two separate histograms are overlaid in each panel (Figs. 7e, f), one corresponding to the thermal fluctuations of a free cantilever (hatched bars) and the other to those of a cantilever linked to the surface via a selectin-ligand bond (gray bars). The differences between the two histograms are greater for L-selectin (Fig. 7e) than for P-selectin, (Fig. 7f), resulting in a more distinct separation of the two subpopulations in the former case than the latter because restraining the cantilever tip by the stiffer L-selectin increases the system spring constant more than the softer P-selectin. Using Eq. (12), the respective molecular spring constants for L-selectin and P-selectin can be determined from the differences in the peak locations of the two histograms from the respective panels. However, there are significant overlaps between the subpopulations under the two peaks due to the small differences in the spring constants of the free and bound cantilevers. This prevents the events of bond formation and dissociation from being detected reliably with sufficient temporal resolution, i.e., without averaging over long periods.

This difficulty can be overcome by using softer force probes with much smaller spring constants, such as those in optical tweezers or BFP.[1] The basic experimental protocol consists of the following cycle. The piezo translator brings the receptor-coated target bead to briefly contact with the ligand-coated probe bead, retracts it to a desired position with sub-nanometer precision, holds it there for a given duration, and returns it to original position. This cycle is repeated many times to acquire an ensemble of data for statistical analysis as in the adhesion frequency assay. The position of the probe bead is continuously recorded and analyzed for detection of events of formation and dissociation of receptor–ligand bonds.[1]

Two such test cycles are exemplified (Figs. 8a, b) for PSGL-1 interacting with L- and P-selectin, respectively. The BFP probe was initially pushed 150 nm by the target, returned to ~0 nm after the target was retracted and held to allow contact with the probe via thermal fluctuations but not by compression, and returned to ~0 nm (Fig. 8a) when the target was retracted again or pulled ~90 nm away by the retracting target then springing back to ~0 nm after adhesion between the probe and target was ruptured (Fig. 8b). Thermal fluctuations were measured by a sliding standard deviation of 15 consecutive points from the time course data (Figs. 8c, d). For a BFP spring constant of $k_p = 0.15$ pN/nm, an expected standard deviation of ~5.2 nm is predicted from the equipartition theorem for a free probe at room temperature (Eq. 8). Pressing the target against the probe suppressed the thermal fluctuations. Nonrandom longdistance travels resulted in artificially large sliding standard deviations when the probe was pushed or pulled by the target. After discarding these, three intervals (arrows) were still clearly seen in Fig. 8a where thermal fluctuations were lower than 3 nm (horizontal solid line in Figs. 8c and 8d, which is a set threshold of one standard deviation lower than that expected for a free probe when the probe was neither pushed nor pulled), suggesting the presence of a bond in these intervals. Indeed, the mean deflections in these periods were shifted upward due to bond formation across a mean gap distance that was slightly larger than the length of the L-selectin/PSGL-1 complex. The threshold method also allowed determination two periods in Fig. 8d in which a bond was present despite the fact that no upward shift of the mean deflection was observed in Fig. 8b, presumably because the mean gap distance between the two surfaces was no larger than the length of the L-selectin/PSGL-1 complex. The suggested absence or presence of a bond immediately prior to the target retraction was confirmed by the observation that the probe was not (Fig. 8a) or was (Fig. 8b) pulled by the retracting target.

Figure 8 is similar to Fig. 7; however, the much softer spring constant of the BFP compared to AFM resulted in clear changes in the displacement fluctuations when a bond is formed or dissociates (Figs. 8a, b compared to Figs. 7a, b), which manifests as a sudden decrease or increase in the standard deviations (Figs. 8c, d compared to Fig. 7c, d), enabling us to pinpoint the time when bond formation or dissociation occurs even when the force probe is placed so

close to the target that bond dissociation does not result in a significant shift in the mean displacement (Fig. 8b compared to Fig. 8a and Figs. 7a, b). The two peaks in each of the standard deviation histograms corresponding to the free and bound force probe are clearly separated with minimal overlaps (Figs. 8e, f compared to Figs. 7e, f). The amount of left shift of the displacement standard deviation resulted from bond formation is smaller for P-selectin than for L-selectin, consistent with the fact that P-selectin has a smaller molecular spring constant than L-selectin. This suggests that the thermal fluctuation assay can distinct the type of bonds in addition to identifying the bond formation and dissociation events.

The correlation (or lack thereof) between the two methods of determining the presence of a bond—by the target pulling during its retraction and by the reduced thermal fluctuations immediately prior to the retraction—can be used to test the reliability of the thermal fluctuation method to determine the presence of a bond at a particular moment. In 725 tests similar to those shown in Fig. 8, Chen *et al.*[1] found ~10% too close to call because their thermal fluctuations immediately prior to the target retraction were in between the upper and lower bounds they chose to separate a free probe from a probe linked to the target by a bond (e.g., in the level similar to those indicated by arrowhead in Fig. 8a). In the remaining 90% of the tests, >96% of the times the thermal fluctuation method reported correctly either having or not having a bond as confirmed by the pulling method (Fig. 9, two diagonal bars). False positive (events scored as having a bond by the thermal fluctuation method but not confirmed by the pulling method) and false negative (events scored as not having a bond by the thermal fluctuation method but shown to have a bond by the pulling method) were <3.5% (Fig. 9, two off-diagonal bars). These results support the reliability of determining bond formation and dissociation events based on the reduction and resumption of thermal fluctuations.

The ability to pinpoint when bond formation and dissociation take place enables measurement of 2D receptor–ligand binding kinetics. The period from the instant of dissociation of an existing bond to the instant of formation of the next bond is the waiting time t_w and the period from the instant of bond formation to the instant of bond dissociation is the bond lifetime t_l. A pooled collection of waiting times can be analyzed by the first-order kinetics of irreversible association of single bonds:

$$P_a = 1 - \exp(-m_r m_l A_c k_{+1} t_w) \tag{13}$$

$1 - P_a$ is the probability for no bond to form during the interval $[0, t_w]$. Taking the natural log of $(1 - P_a)$ linearizes the exponential waiting time distribution given by Eq. (13). The negative slope of the ln(# of events with a waiting time $\geq t$) vs. t_w plot provides an estimate for $m_r m_l A_c k_{+1}$ (Fig. 10a). Similarly, a pooled collection of bond lifetimes can be analyzed by the first-order kinetics of irreversible dissociation of single bonds:

$$P_b = \exp(-k_{-1} t_l), \tag{14}$$

where P_b is the probability for a bond formed at time 0 to remain bound at time t_l. Taking the natural log of P_b linearizes the exponential bond lifetime distribution given by Eq. (14). Thus, the negative slope of the ln(# of events with a lifetime $\geq t$) vs. t_l plot provides an estimate for k_{-1} (Fig. 10b). Note that Eqs. (13) and (14) each contains only a single parameter, which makes their respective curve-fitting of the waiting time distribution (Fig. 10a) and lifetime distribution (Fig. 10a) more robust and the best-fit parameters more reliable.

If the negative slopes of the linear fits to the data in Figs. 10a and 10b indeed represent respective cellular on-rates and off-rates, then the former should increase linearly with, and the latter should be independent of, the site densities of the receptors and ligands, provided that

observed interactions reflect predominately single bonds. Chen *et al.* tested this prediction by measuring L-selectin-PSGL-1 interaction kinetics using four different site densities.[1] The cellular association rate constant, $m_r m_l A_c k_{+1}$, was found to be proportional to the site densities of L-selectin and PSGL-1 (Fig. 11a), as expected from second-order forward reaction (Eqs. 4 and 13). The slope of the linear fit in Fig. 11a gives the average on-rate. The off-rate constant was found to be independent of the site densities (Fig. 11b), as expected from Eq. (14).

The validity of the thermal fluctuation assay can be tested by the sensitivity of the kinetic parameters estimated to the molecular interactions assayed, e.g., L-selectin vs. PSGL-1 and P-selectin vs. PSGL-1. Histograms of waiting times and lifetimes of these two interactions at comparable site densities are compared in Figs. 10a and 10b. It clearly shows that P-selectin has faster on-rate, but slower off-rate, to PSGL-1 than L-selectin. The kinetic rates are compared in Fig. 11c, which are consistent with previous finding that P-selectin[8] has much higher affinity and slower off-rate to PSGL-1 than L-selectin.[9]

The thermal fluctuation method can be further validated by comparing the 2D kinetic rates measured by this method with those measured by the adhesion frequency assay,[2] which has been extensively used to determine many receptor–ligand interactions. As described in the previous section, rather than measuring rupture forces, the adhesion frequency assay estimates the likelihood of adhesion, or adhesion probability, P_a, from the frequency of adhesion enumerated from a large number of repeated controlled contacts. P_a is related to the contact time t_c through a probabilistic model described by Eq. (6) in adhesion frequency assay session. [2]

Using the same BFP, same reagents, same site densities, and experiments prepared the same way as those in the thermal fluctuation method, Chen *et al.*[1] measured adhesion frequencies in a range of contact durations for L-selectin (△) or P-selectin (○) interacting with PSGL-1. Theoretical adhesion frequencies as functions of contact time were predicted (curves) by Eq. (6) using the kinetic rates from Fig. 11c and molecular densities measured from independent experiments. It is evident that the predictions agree with the data reasonably well for both the L-selectin and P-selectin cases (Fig. 12), further supporting the validity of the thermal fluctuation method.

Summary

In this paper, we have reviewed two assays for measuring two-dimensional binding kinetics of a low number of receptor–ligand interactions. The 2D nature allows reaction kinetics to be assayed mechanically. That such binding is mediated by a low number of molecular interactions requires ultrasensitive force techniques and a probabilistic kinetic framework for analysis. These assays measure 2D force-free on- and off-rates. Off-rates of biomolecular interaction are known to be regulated by applied force,[6,11] which is treated by other papers in this thematic issue. Two-dimensional kinetics of a large number of molecular interactions can also be assayed using a recently developed fluorescence-based assay.[13,17] Collectively, these assays provide useful methodologies for studying molecular interactions across two apposing surfaces.

Acknowledgments

We thank our coworkers of references Chen *et al.*[1] and Huang *et al.*[5] who contributed the original data that are discussed here. This work was supported by National Institutes of Health Grants AI38282, AI44902, and HL091020. W.C. is a Predoctoral Fellowship recipient of the American Heart Association (Greater Southeast Affiliate).

References

1. Chen W, Evans EA, McEver RP, Zhu C. Monitoring receptor-ligand interactions between surfaces by thermal fluctuations. Biophys J 2008;94(2):694–701. [PubMed: 17890399]
2. Chelsa SE, Selvaraj P, Zhu C. Measuring two-dimensional receptor-ligand binding kinetics by micropipette. Biophys J 1998;75(3):1553–1572. [PubMed: 9726957]
3. Evans E, Berk D, Leung A. Detachment of agglutinin-bonded red blood cells. I. Forces to rupture molecular-point attachments. Biophys J 1991;59(4):838–848. [PubMed: 2065188]
4. Evans E, Heinrich V, Leung A, Kinoshita K. Nano- to microscale dynamics of P-selectin detachment from leukocyte interfaces. I. Membrane separation from the cytoskeleton. Biophys J 2005;88(3):2288–2298. [PubMed: 15653718]
5. Huang J, Edwards LJ, Evavold BD, Zhu C. Kinetics of MHC-CD8 interaction at the T cell membrane. J Immunol 2007;179(11):7653–7662. [PubMed: 18025211]
6. Marshall BT, Long M, Piper JW, Yago T, McEver RP, Zhu C. Direct observation of catch bonds involving cell-adhesion molecules. Nature 2003;423(6936):190–193. [PubMed: 12736689]
7. Marshall BT, Sarangapani KK, Wu J, Lawrence MB, McEver RP, Zhu C. Measuring molecular elasticity by atomic force microscope cantilever fluctuations. Biophys J 2006;90(2):681–692. [PubMed: 16258054]
8. Mehta P, Cummings R, McEver R. Affinity and kinetic analysis of P-selectin binding to P-selectin glycoprotein ligand-1. J Biol Chem 1998;273(49):32506–32513. [PubMed: 9829984]
9. Nicholson MW, Barclay AN, Singer MS, Rosen SD, van der Merwe PA. Affinity and kinetic analysis of L-selectin (CD62L) binding to glycosylation-dependent cell-adhesion molecule-1. J Biol Chem 1998;273(2):763–770. [PubMed: 9422729]
10. Piper JW, Swerlick RA, Zhu C. Determining force dependence of two-dimensional receptor-ligand binding affinity by centrifugation. Biophys J 1998;74(1):492–513. [PubMed: 9449350]
11. Sarangapani KK, Yago T, Klopocki AG, Lawrence MB, Fieger CB, Rosen SD, McEver RP, Zhu C. Low force decelerates L-selectin dissociation from P-selectin glycoprotein ligand-1 and endoglycan. J Biol Chem 2004;279(3):2291–2298. [PubMed: 14573602]
12. Thoumine O, Kocian P, Kottelat A, Meister JJ. Short-term binding of fibroblasts to fibronectin: optical tweezers experiments and probabilistic analysis. Eur Biophys J 2000;29(6):398–408. [PubMed: 11081401]
13. Tolentino TP, Wu J, Zarnitsyna VI, Fang Y, Dustin ML, Zhu C. Measuring diffusion and binding kinetics by contact area FRAP. Biophys J 2008;95(2):920–930. [PubMed: 18390627]
14. Williams TE, Nagarajan S, Selvaraj P, Zhu C. Quantifying the impact of membrane microtopology on effective two-dimensional affinity. J Biol Chem 2001;276(16):13283–13288. [PubMed: 11278674]
15. Wong W, Halvorsen K. The effect of integration time on fluctuation measurements: calibrating an optical trap in the presence of motion blur. Opt Express 2006;14(25):12517–12531. [PubMed: 19529687]
16. Wu J, Fang Y, Yang D, Zhu C. Thermo-mechanical responses of a surface-coupled AFM cantilever. J Biomech Eng 2005;127(7):1208–1215. [PubMed: 16502663]
17. Wu J, Fang Y, Zarnitsyna VI, Tolentino TP, Dustin ML, Zhu C. A coupled diffusion-kinetics model for analysis of contact area FRAP experiment. Biophys J 2008;95(2):910–919. [PubMed: 18390628]
18. Zarnitsyna VI, Huang J, Zhang F, Chien YH, Leckband D, Zhu C. Memory in receptor-ligand-mediated cell adhesion. Proc Natl Acad Sci USA 2007;104(46):18037–18042. [PubMed: 17991779]
19. Zhu C, Long M, Chesla SE, Bongrand P. Measuring receptor/ligand interaction at the single-bond level: experimental and interpretative issues. Ann Biomed Eng 2002;30(3):305–314. [PubMed: 12051616]

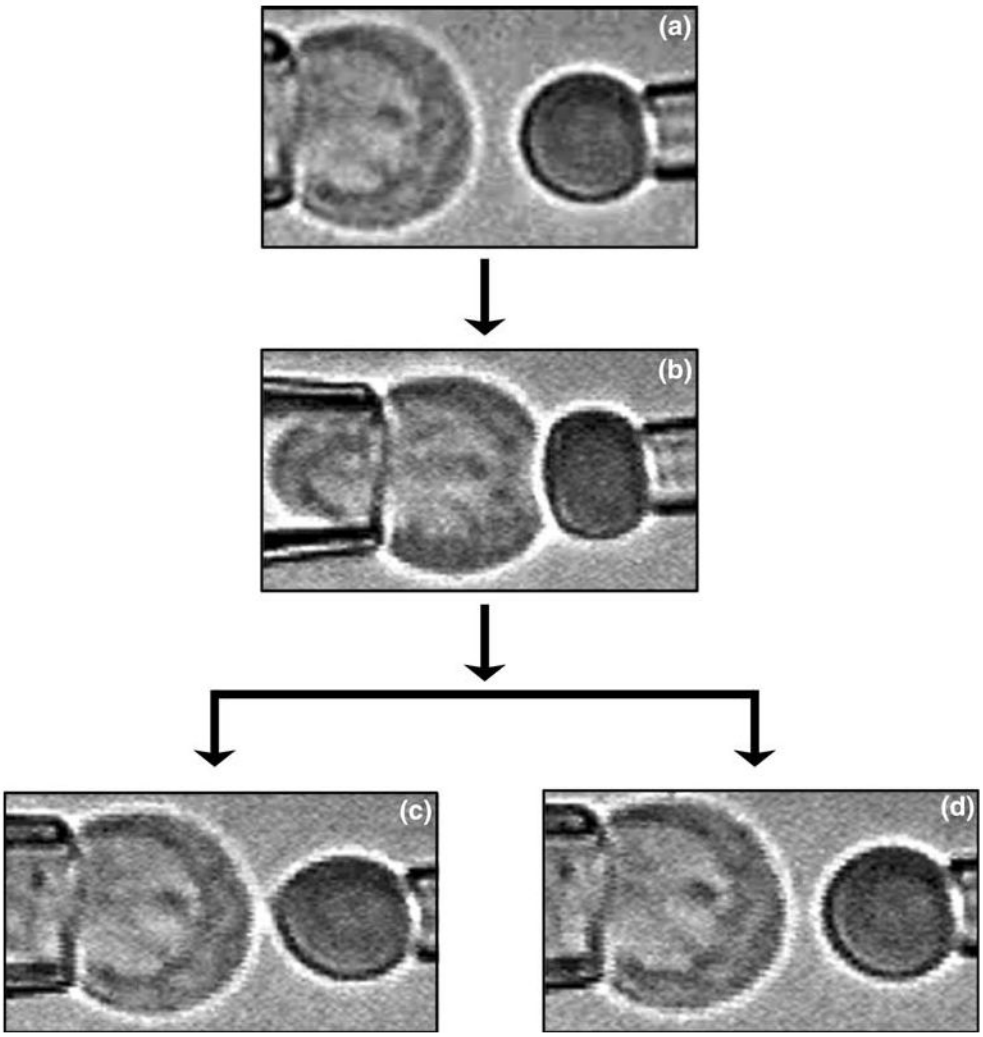

FIGURE 1.

Micropipette-aspirated RBC adhesion sensor. A micropipette-aspirated T cell (a, *left*) was driven by a piezoelectric translator to make a controlled contact with a RBC coated with MHC held stationary by another pipette (b, *right*). At the end of the contact period, the computer-driven translator retracted the pipette to the starting position. An adhesion, if present, would result in elongation of the RBC upon its retraction, enabling visual detection of the adhesion (c). The RBC membrane would retract away from the T cell surface smoothly if there was no adhesion (d). Reproduced from Huang *et al.*[5] with permission.

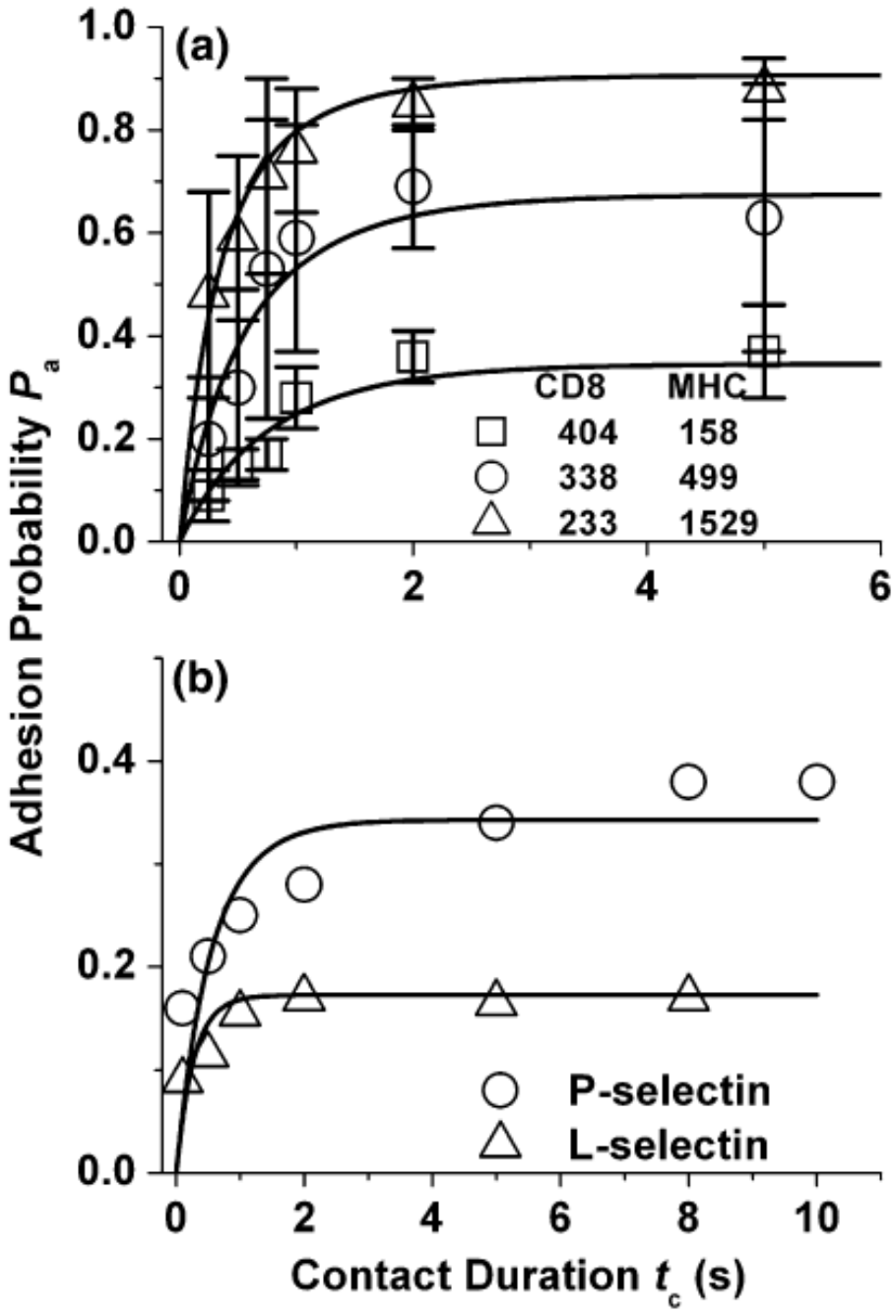

FIGURE 2.

Adhesion frequency vs. contact duration plots. (a) Data (points) measured using three sets of site densities (indicated), each obtained from 15 to 29 pairs of CD8+ T cells and noncognate pMHC-coated RBCs contacting 50 times each, were presented as mean ± SEM at each contact duration. Equation (6) was globally fit (curves) to all three data sets with $k_{-1} = 1.12 \pm 0.15$ s^{-1} and $A_cK_a = 6.66 \pm 0.36 \times 10^{-6}$ μm.[3] Reproduced from Huang *et al.*[5] with permission. (b) Endoglycan-Ig captured on an AFM cantilever tip precoated with protein G[12] was driven to repeatedly contact L-selectin (△) or P-selectin (○) reconstituted in glass-supported lipid

bilayer.[6] Data (points) were fitted (curves) by Eq. (6) with $k_{-1} = 3.55\ s^{-1}$ and $m_r m_l A_c K_a = 0.19$ for L-selectin and $k_{-1} = 1.57\ s^{-1}$ and $m_r m_l A_c K_a = 0.42$ for P-selectin.

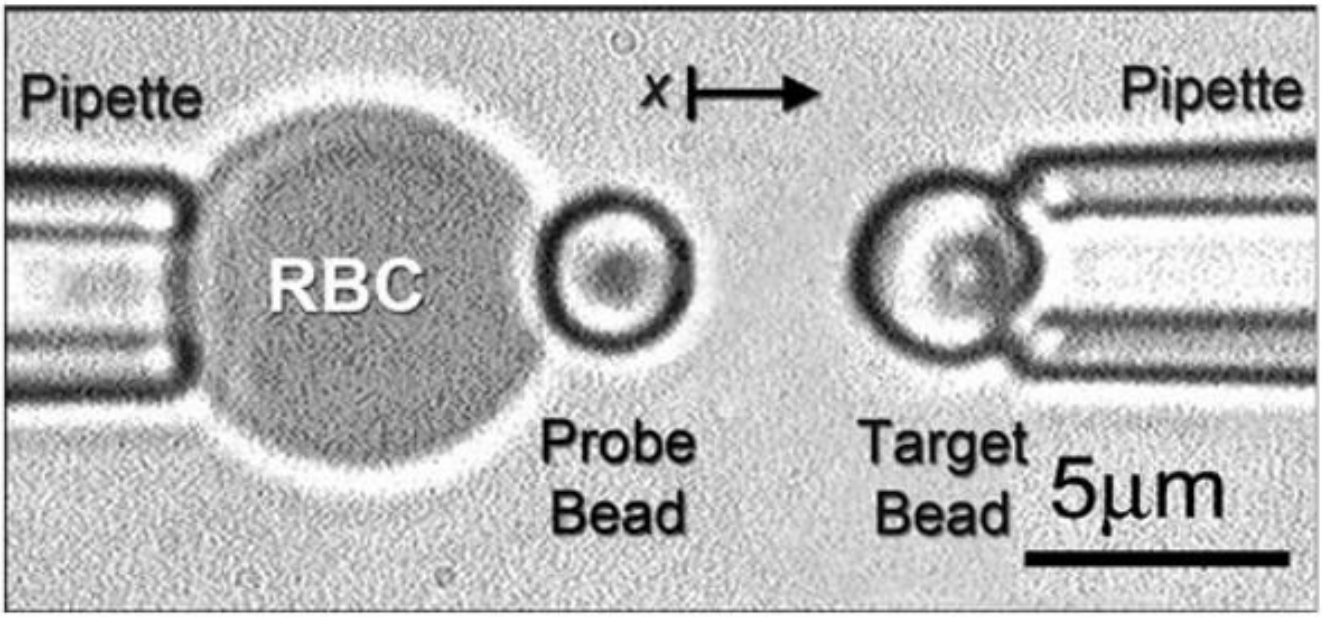

FIGURE 3.

Photomicrograph of a BFP. A micropipette-aspirated RBC with a bead (probe) glued to its apex (*left*) was aligned against another bead (target) aspirated by another pipette (*right*). The right pipette was driven by a computer-programmed piezoelectric translator to move in a repeated approach-push-retract-hold-return test cycle. The left pipette was held stationary but the position of the probe was tracked by a high-speed camera and analyzed by advanced tracking software.

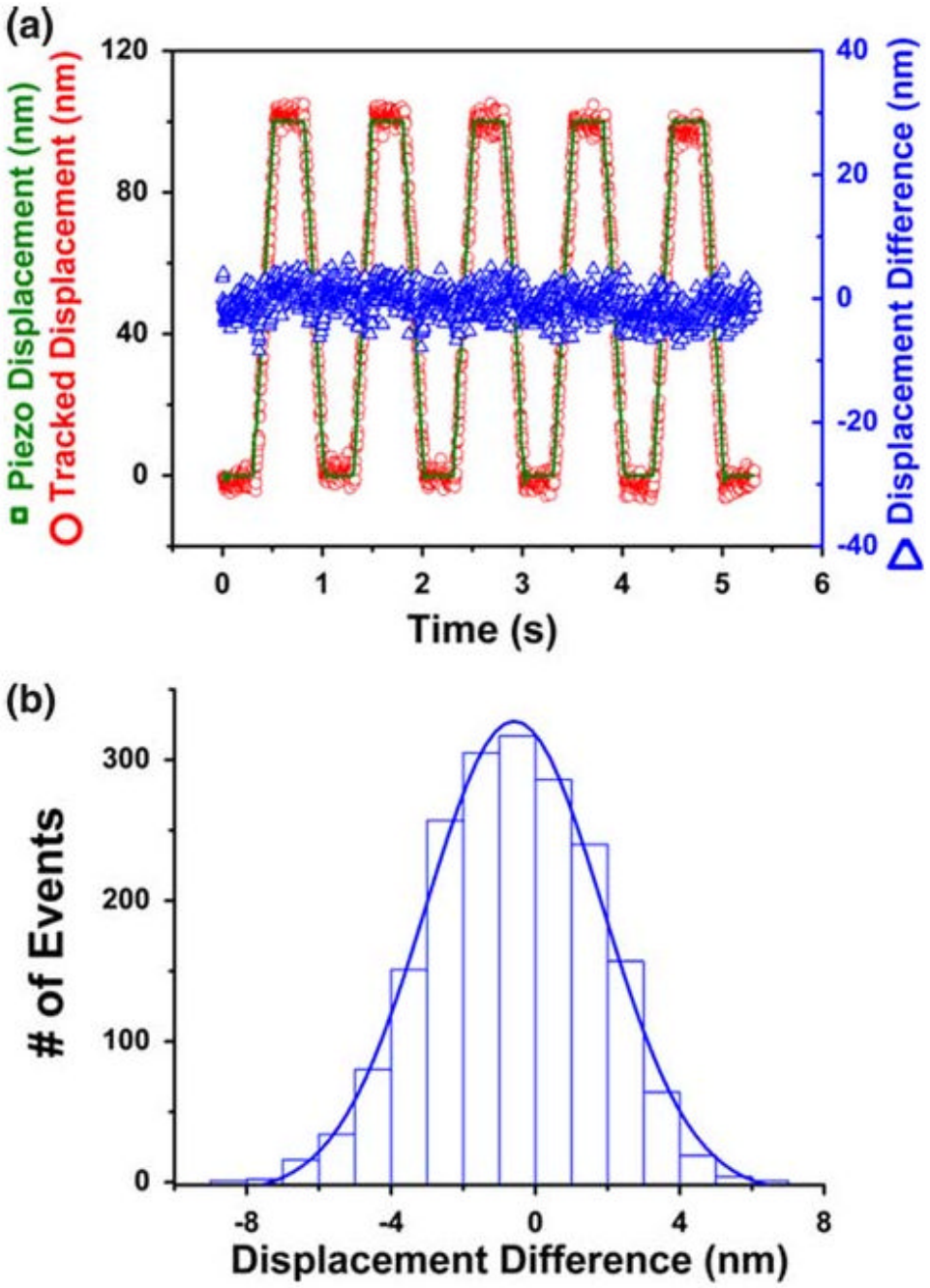

FIGURE 4.

Characterization of the tracking precision of BFP. (a) Comparison of the piezo displacements (green, □) and the tracked displacements (red, ○). The differences between them are shown as blue (△). (b) Histogram (bars) of the differences between the piezo and tracked displacements. It is fitted by a Gaussian distribution (curve).

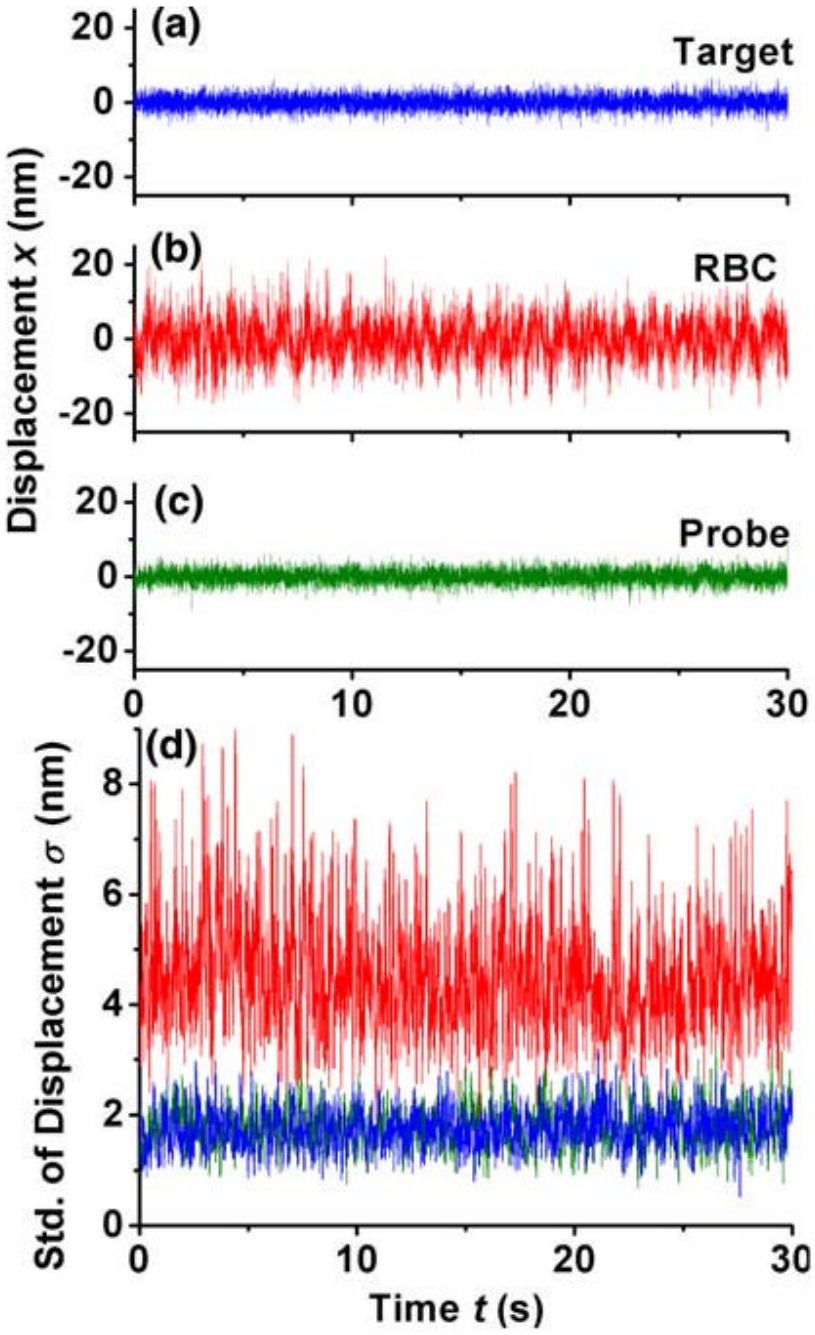

FIGURE 5.

Illustration of thermal fluctuations. Tracked displacements of the target pipette (a), the force probe (b), and the probe pipette (c) over time during which both pipettes were held stationary. (d) Comparison of the 15-point sliding standard deviations of the fluctuating displacements in a–c (color-matched).

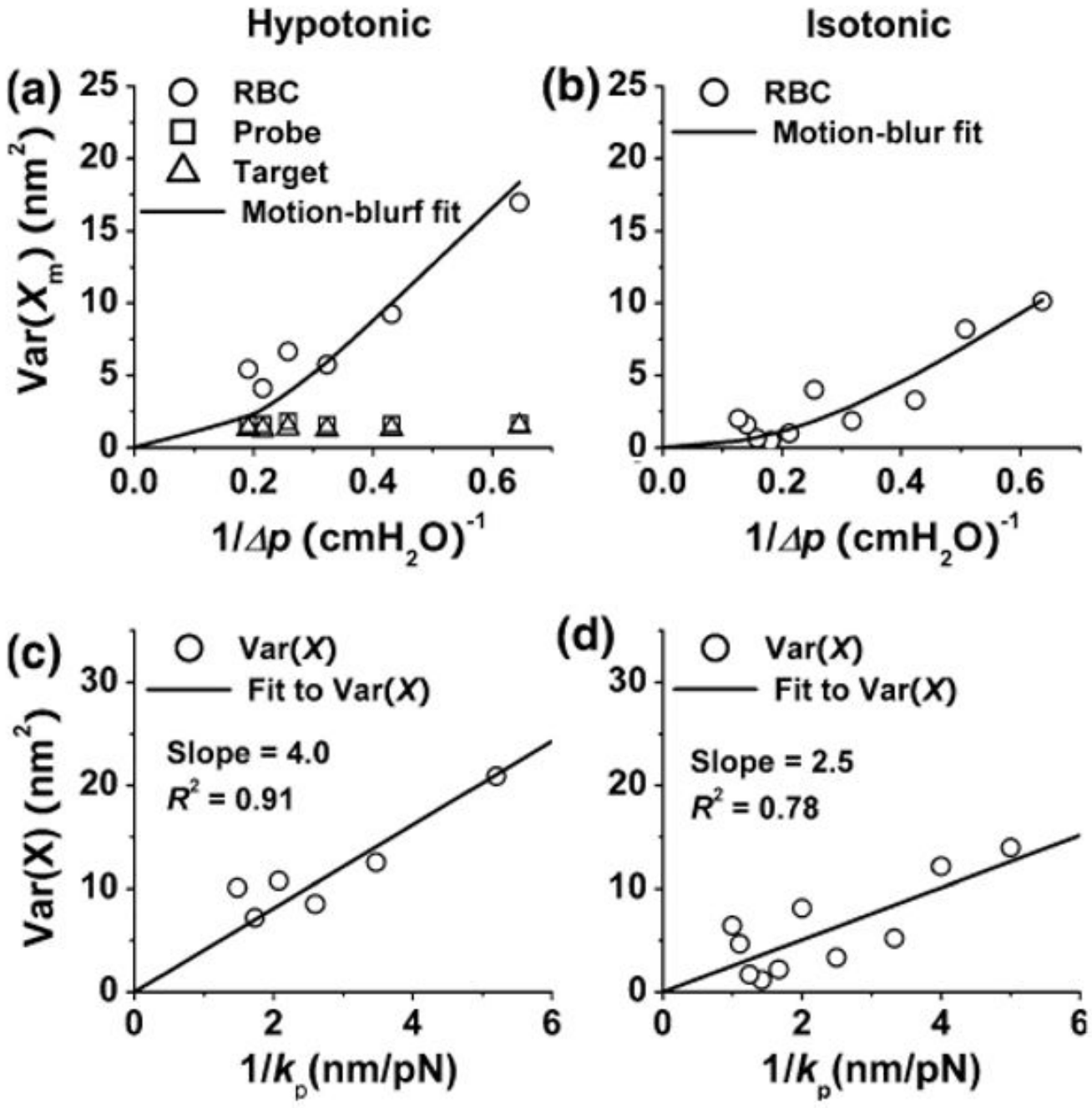

FIGURE 6.

Calibration of BFP spring constant. (a, b) The background-subtracted drift-free variance var (X_m) of a BFP force probe (○) is plotted vs. reciprocal suction pressure $1/\Delta p$ under which the fluctuating displacements were measured in hypotonic (a) or isotonic (b) condition and fitted by the motion-blur model Eq. (11) (curve). The variances of the target bead (△) and the probe pipette (□) are also plotted in (a), which serve as the background. (c, d) The motion-blur corrected variance var(X) (○) is plotted vs. $1/k_p$ calculated from Eq. (11) using parameters from the experiments under which the fluctuating displacements were measured in hypotonic (c) or isotonic (d) condition and fitted by a straight linear that passes the origin.

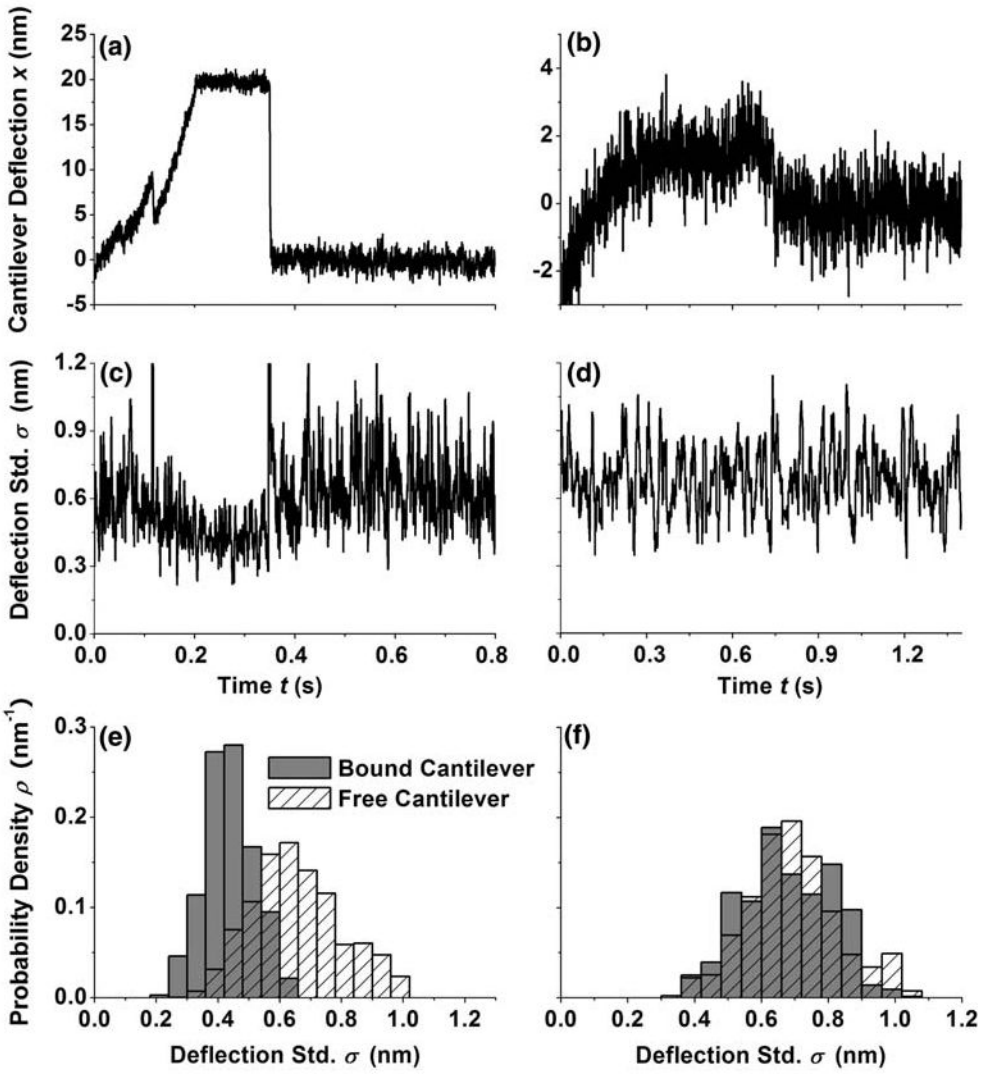

FIGURE 7.

Comparison of thermal fluctuations of bound and free cantilever. Cantilever deflection *x* vs. time *t* curve of L-selectin/ PSGL-1 interaction (a) or P-selectin/endoglycan interaction (b) in experiment that measures bond lifetime at a constant force. (c, d) Sliding standard deviations σ of 15 consecutive points of the cantilever deflection data in (a) and (b), respectively. (e, f) Histograms of the σ data in (c) and (d), respectively.

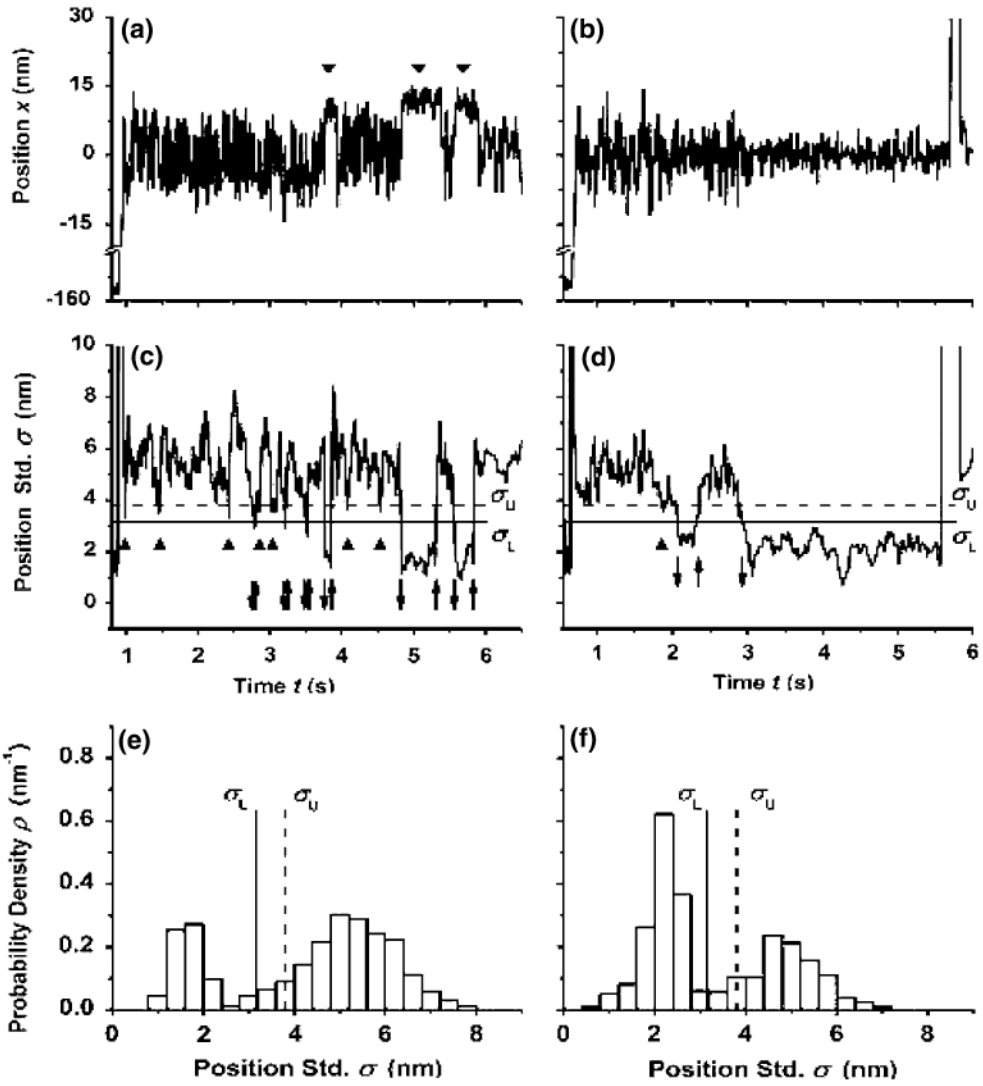

FIGURE 8.

Thermal fluctuation method. (a, b) Horizontal position *x* of the right edge of the probe is plotted vs. time *t* for a representative test cycle measuring interactions of PSGL-1 coated on the probe with L- (a) or P-selectin (b) coated on the target. Two periods of high positions in (a) are indicated by arrowheads. (c, d) Sliding standard deviations σ of 15 consecutive points of the position data in (a) and (b), respectively. (e, f) Histograms of the σ data in (c) and (d) (bars), respectively. The vertical dashed line $\sigma_U = 3.8$ nm on each panel is one standard deviation (1.3 nm) to the left from the peak at 5.1 nm. The vertical solid line $\sigma_L = 3.15$ nm on each panel is 1.5 standard deviation to the left from the same peak. These thresholds are marked in (c) and (d) as horizontal lines to identify bond association/dissociation events, which are marked by the respective down and up arrows. Arrowheads indicate intervals deemed indeterminate for whether they corresponded to free or bound probes because data lay between the two thresholds. Reproduced from Chen *et al.*[1] with permission.

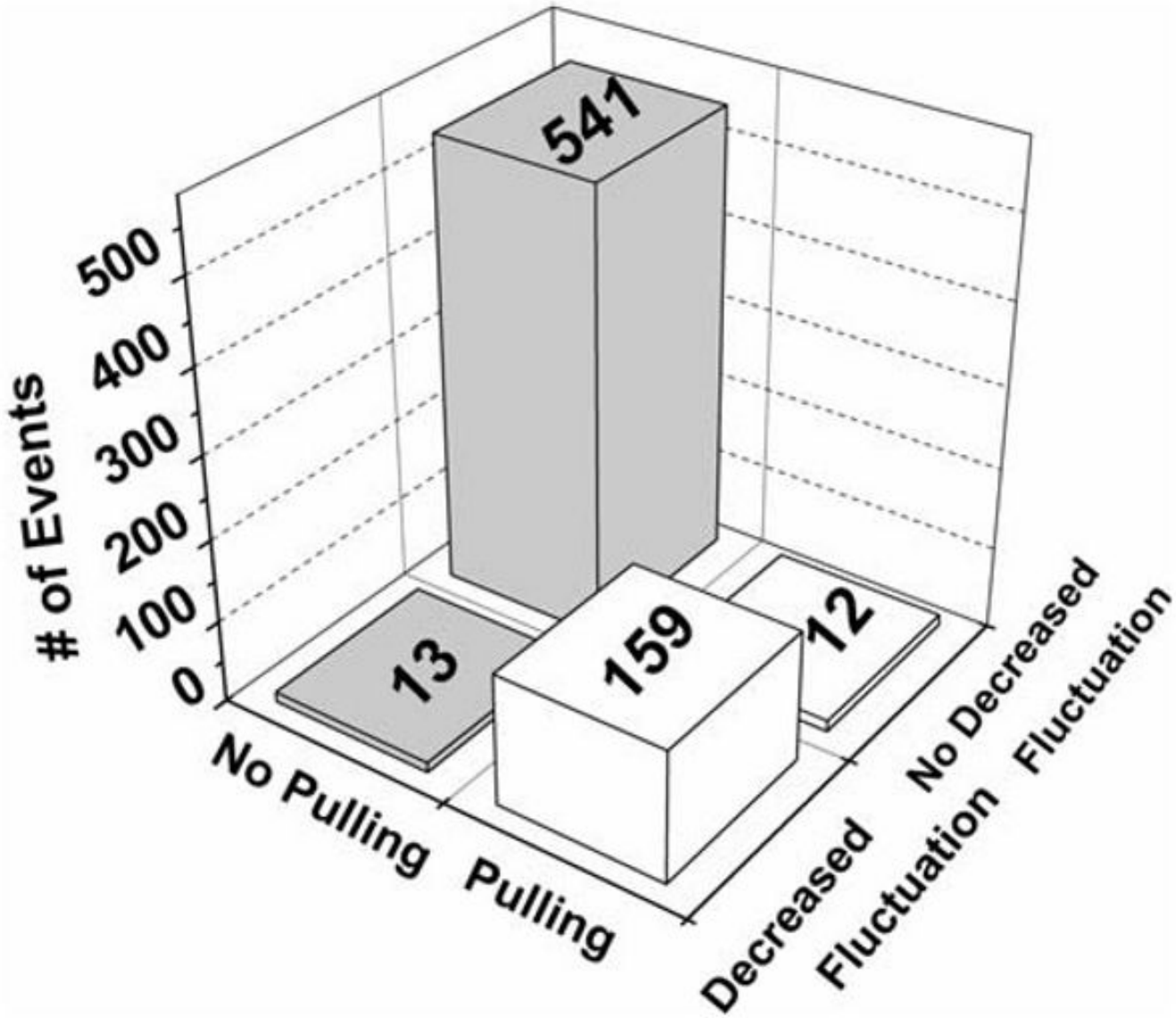

FIGURE 9.
Correlation between two methods for determining the presence of a bond. Reproduced from Chen *et al.*[1] with permission.

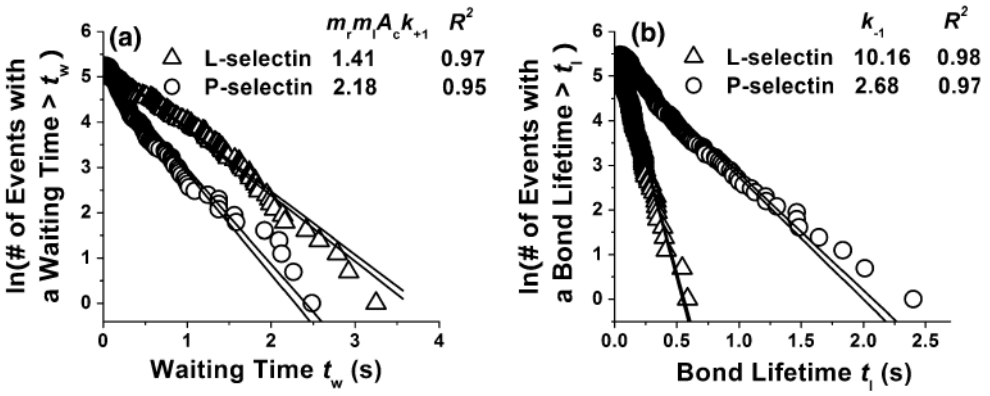

FIGURE 10.

Exponential distributions of pooled bond waiting times (a) and bond lifetimes (b) of PSGL-1 interacting with L- and P-selectin, respectively. Reproduced from Chen *et al.*[1] with permission.

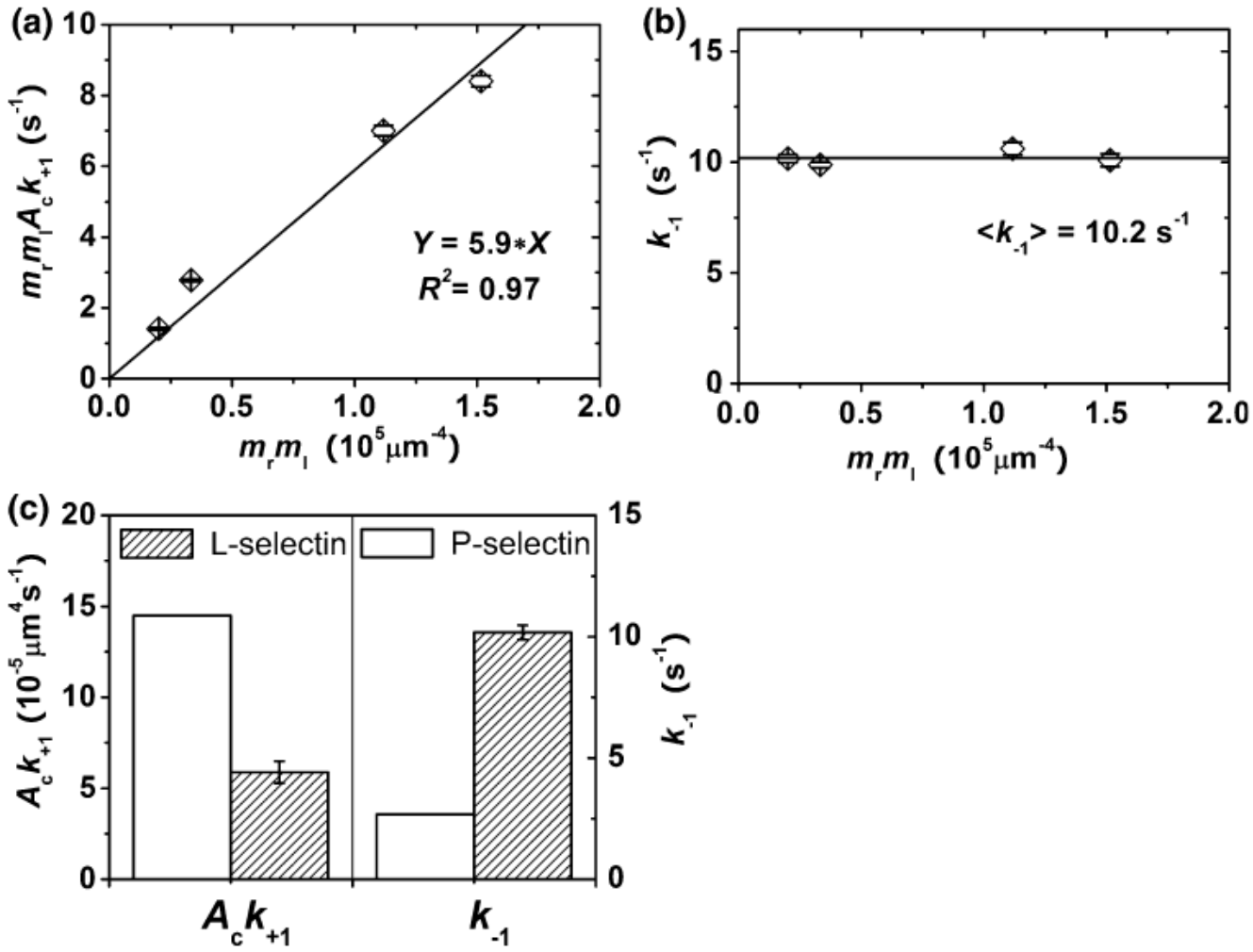

FIGURE 11.

Kinetic parameters. Cellular on-rate (a) and off-rate (b) were plotted vs. product of the site densities of the interacting molecules, L-selectin and PSGL-1. Data (points, error bar = 95% confident interval) were respectively fitted by a straight line that passed the origin (a) to estimate a molecular 2D effective on-rate $\langle A_c k_{on} \rangle$ (best-fit equation and R^2 were indicated) or by a horizontal line (b) to estimate the average off-rate $\langle k_{off} \rangle$ (indicated). (c) Comparison of kinetic rates of PSGL-1 interacting with L-selectin and P-selectin. Reproduced from Chen *et al.*[1] with permission.

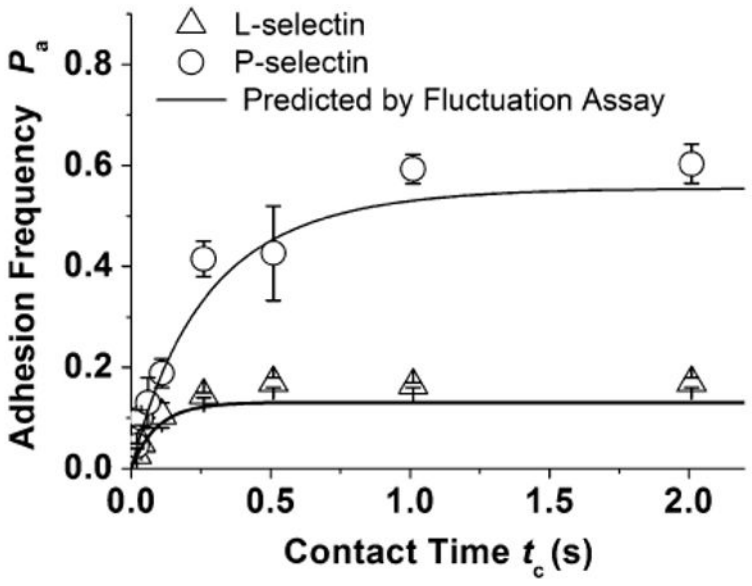

FIGURE 12.

Comparison between theory and experiment. Frequencies of adhesion mediated by PSGL-1 interacting with L-selectin (△) or P-selectin (○) were measured at indicated contact times. Theoretical adhesion frequencies as functions of contact time were predicted (curves) by Eq. (6) using the kinetic rates from Fig. 11c and molecular densities measured from independent experiments ($m_r m_l$, = 0.2 and $0.15 \times 10^5\ \mu m^{-4}$ for the L- and P-selectin cases, respectively). Reproduced from Chen *et al.*[1] with permission.